HYDRAULIC FRACTURING PROPAGATION MECHANISM DURING SHALE GAS RESERVOIR STIMULATION THROUGH HORIZONTAL WELL

Tian-hui Ma, Quan-ao Wu, Chun-an Tang, Hong-yuan Liu

The fracture pattern of rock mass in shale gas reservoirs is one of the main factors affecting the efficiency of hydraulic fracturing. In this paper, physical experiments and numerical modelling were conducted to systematically investigate the effect of the in-situ stress and perforation angle on the hydraulic fracture initiation pressure and location, fracture propagation, and fracture pattern in a horizontal well drilled by Sinopec Corp. in Luojia area of Shengli Oilfield. A total of six different in-situ stress combinations and eight different perforation angles were considered for the stratified rock mass during the hydraulic fracturing. A summary of the fracture initiations and propagation, and the final fracture patterns induced by the hydraulic fracturing in the stratified rock masses reveals that, for the stratified rock masses with the same perforation angle, the larger the in-situ stress ratio (i.e. lower maximum horizontal principal stress when the vertical stress remains constant) is, the lower hydraulic pressure is required for hydraulic fracturing initiation and propagation. Moreover, it is found that, for the stratified rock mass under the same stress ratio, the hydraulic fracturing pressure in the case with a perforation angle of 30° is higher than that in all other cases. Furthermore, it is noted that the effect of the stratification on the hydraulic fracturing becomes weaker with the in-situ stress ratio increasing. It is finally concluded that the results from this study can provide important theoretical guidance for improving the hydraulic fracturing design in order to ensure the effective shale gas reservoir stimulations.

Keywords: fracture pattern; horizontal well; hydraulic fracturing; in-situ stress; perforation angle

Mehanizam za propagaciju hidrauličkog frakturiranja tijekom stimuliranja naslaga naftnih škriljaca kroz horizontalnu bušotinu

Način razlamanja stijenske mase u naslagama naftnih škriljaca jedan je od glavnih čimbenika koji djeluju na učinkovitost hidrauličkog frakturiranja (frakiranja). U ovom su radu provedena fizikalna ispitivanja i numeričko modeliranje u svrhu sustavnog ispitivanja učinka in-situ (podzemnog) naprezanja i kuta bušenja na stvaranje tlaka zbog hidrauličkog frakturiranja, širenje razlamanja i način razlamanja u horizontalnoj bušotini naftnog nalazišta Shengli u Luojia pokrajini, u izvođenju Sinopec Corp. Ukupno je razmatrano šest različitih in-situ kombinacija naprezanja i osam različitih kutova bušenja slojevite stijenske mase tijekom hidrauličkog frakturiranja. Sažetak nastanka i širenja pukotine te završni oblici pukotina nastalih hidrauličkim frakturiranjem u slojevitim stijenskim masama otkrivaju da kod stratificiranih stijena s istim kutom bušenja, što je veći in-situ omjer naprezanja (t.j. niže maksimalno horizontalno osnovno naprezanje pri konstantnim vertikalnim naprezanjem), potreban je niži hidraulički tlak za poticanje i širenje hidrauličkog frakturiranja. Štoviše, ustanovljeno je da je kod stratificirane stijenske mase pri istom omjeru naprezanja, tlak hidrauličkog frakturiranja, u slučaju kad je kut bušenja 30°, veći nego u svim drugim slučajevima. Nadalje, zapaženo je da učinak stratifikacije na hidrauličko frakturiranje postaje slabiji s porastom in-situ omjera naprezanja. Konačno je zaključeno da rezultati ove analize mogu biti važan teorijski pokazatelj u poboljšanju oblikovanja hidrauličkog frakturiranja kako bi se osiguralo učinkovito stimuliranje naslaga naftnih škriljaca.

Ključne riječi: hidrauličko frakturiranje; horizontalna bušotina; in-situ naprezanje; kut bušenja; način razlamanja

1   Introduction

Shale gas refers to the natural gas accumulated in organic-rich, dark-coloured or high-carbon shale mainly in the form of adsorbed or free gas [1]. Shale gas has a very wide application prospect, which is extremely important in the countries dominated by this type of energy resource. Shale gas is widely distributed worldwide, with a total storage volume of $4,56 \times 10^{14}$ m³, which is half of the petroleum gas resource in the world [2, 3].

As the shale gas reservoir is usually of low porosity and low permeability, only very small number of natural reservoirs can be directly used for production. In fact, most shale gas wells need to be subjected to a series of stimulations before the desired yield can be achieved [4]. Hydraulic fracturing is the most effective shale gas reservoir stimulation method and, correspondingly, the hydraulic fracturing theory and practice have been further advanced.

The hydraulic fracturing technique was first successfully applied in Kansas State, USA, in 1947. The classical hydraulic fracturing method was then proposed by Hybbert and Willis in 1957 [4, 5]. With development over 60 years, the hydraulic fracturing technique has now been widely applied in underground engineering, such as the exploitation of petroleum, geotherm and coalbed methane, disposal of nuclear waste and measurement of geostresses. Some research achievements have been made in terms of both theory and practice. Hydraulic fracturing has become an important technical means to improve the well output and recovery efficiency in low-permeability reservoirs during the exploitation of oil and gas fields [6].

Especially in recent years, driven by the horizontal well staged hydraulic fracturing, great success has been achieved for unconventional natural gas exploitation in extremely low-permeability shale reservoirs in the Granada area of the U. S. The yielded shale gas reached $1720,0 \times 10^8$ m³ in the U.S. in 2011, which was much more than the total natural gas produced in China in 2011($1025,3 \times 10^8$ m³) [7].

The pattern of hydraulic fracture is one of the main factors affecting the efficiency of hydraulic fracturing: for cost-effective fracturing, the fractures should propagate in the reservoir bed as far as possible and meanwhile the fracture propagation through pervious layer or low-pressure permeable layer should be prevented [8]. In traditional hydraulic fracturing theory, the hydraulic fractures far away from the well are considered as the symmetrical double-wing cracks propagating perpendicularly to the direction of minimum principal in-situ stress. During recent years, many researchers have realized that hydraulic fractures can propagate in much

more complex patterns. Warpinski et al. [9÷11] found, for the first time, that the main fracture and complex branch fractures could propagate simultaneously and proposed the concept of fracture extension zone. With physical model tests, Blanton [12, 13] and Chen et al. [14÷17] found that three cases were possible after the hydraulic fractures intersected with natural fractures, i.e., the hydraulic fractures might penetrate, turn or penetrate and turn at the same time. Mahrer [18] suggested that the natural fractures and hydraulic fractures would together form a fracture network. Later, Beugelsdijk [19] verified the existence of the fracture network by laboratory tests. Fisher et al. [20, 21] and Mawell et al. [22, 23] confirmed the existence of the fracture network in the field of shale gas reservoirs by microseismic monitoring. In sum, hydraulic fractures are the key to the successful modification of shale gas reservoir beds [24].

From the previous researches reviewed above, it can be seen that, till this moment, the primary evaluation on the fracturing efficiency and the fracture propagation law are based on the change of oil and gas yield after fracturing and the experiences in hydraulic fracturing. Moreover, although some achievements have also been made in the numerical simulation of fracture propagation during hydraulic fracturing, these numerical simulations mainly focus on the studies of the static parameters related to hydraulic fracturing such as the fracture pattern and the dimension (length, width and height) of the fractures. Few studies have been conducted on the dynamic parameters of hydraulic fractures, such as the dynamic propagation direction, path and range. Especially, as commented by Sun et al. [6], numerical simulations are seldom reported to investigate the interaction between the hydraulic fractures and the oriented cracks created by perforation and slotting.

In view of the non-systematic and incomplete knowledge on the formation mechanism of fracture network in shale gas reservoir beds, this study took a well drilled by Sinopec Corp. in Luojia area of Shengli Oilfield as an example to conduct a systematic study on the effect of the deviatoric stress and perforation angle on the hydraulic fracture initiation pressure, fracture initiation location, fracture propagation and fracture pattern during hydraulic fracturing [25]. This study can provide important theoretical guidance for improving the reliability of hydraulic fracturing design in stimulating shale gas reservoirs.

2 Computation principle and physical test for obtaining the parameters of hydraulic fractures

2.1 Introduction of computation principle for modelling hydraulic fractures

Natural rock masses are discontinuous, inhomogeneous, inelastic and anisotropic media, which are time-dependent, path-dependent and environment-dependent. Although many theoretical formulas have been derived according to classical mechanics, they are not applicable to the complex engineering rock masses [25]. In many practical engineering projects, rock mass deformation, failure and strength calculated by these idealized formulas are far from the true values. So far, the knowledge on the irregularity, complexity and

nonlinearity of the physical and mechanical properties of the rock mass is still incomplete and relevant issues are yet to be solved. Consequently, many rock mechanics problems cannot be explained and analysed quantitatively or even qualitatively.

Statistics theory has been playing a significant role in the studies on the strength of heterogeneous materials at mesoscopic level. As the macroscopic manifestation of mesoscopic statistical strength, the deformation and failure processes of geological materials can be well explained. Hence, the statistics theory is considered as a rigorous and promising method of studying heterogeneous materials. The strength obtained from the viewpoint of mesoscopic statistics of the heterogeneous material reflects inevitably the overall strength of the heterogeneous material. In this paper, the seepage module of the realistic failure process analysis (RFPA-Flow) is adopted for numerical simulation. The rock homogeneity is realized by assigning the mechanical parameters (elastic modulus, Poisson's ratio, compressive strength, etc.) of the rock according to the Weibull distribution in Eq. (1).

$$\phi(\alpha) = \frac{m}{\alpha_0} \left(\frac{\alpha}{\alpha_0} \right)^{m-1} e^{-\left(\frac{\alpha}{\alpha_0} \right)^m},$$ (1)

where α is the mechanical parameter of meso-elements of a medium (rock); α_0 is the statistical average of mesoscopic mechanical properties; m is the heterogeneity index, and the larger the homogeneous index m, the higher the homogeneous degree is; and $\phi(\alpha)$ is the probability density function of α.

The fluid flow in the medium (rock) of a RFPA-Flow model satisfies the Biot's consolidation theory. The mesoscopic element of the rock medium is assumed to be an elastic-brittle material with a certain residual strength. Its mechanical behaviours during the loading and unloading processes conform to the elastic damage theory. The maximum tensile strength criterion and the Mohr-Coulomb strength criterion are employed as the failure criteria for the elements under tensile and compressive loading conditions, respectively. In the elastic state, the relationship between the stress and permeability coefficient of the material can be described by a negative exponential function in Eq. (2).

$$K_f = K_0 e^{-b\sigma}$$ (2)

where K_0 is the initial permeability coefficient; σ is the normal stress; and b is the coupling parameter.

Under the same loading condition, the seepage behavior in rock mass with growing fractures is different from that with pre-existing fractures. Hence, during the damage process of fractured rock mass, the permeability of the rock mass keeps changing. RFPA-Flow can consider not only the propagation of pre-existing fractures and the initiation of new fractures, but also the seepage-stress-damage coupling effect during the propagations of both two types of fractures. In this way, the numerical simulation can reproduce the coupling behaviour of fluid

and rock during the rock damage and failure process in hydraulic fracturing and the modeling results are more realistic and reasonable, compared with those obtained using other fluid and solid coupling software.

The fundamental equations for modelling the fluid-solid coupling during the rock damage and failure process in hydraulic fracturing using RFPA-Flow are denoted in Eqs. (3) ÷ (6), which include the equilibrium equation in Eq. (3):

$$\frac{\partial \sigma_{ij}}{\partial x_{ij}} + \rho X_j = 0, \ i, j = 1, 2, 3. \tag{3}$$

The geometric equation in Eq. (4):

$$\varepsilon_{ij} = \frac{1}{2}\left(u_{i,j} + u_{j,i}\right), \ \varepsilon_v = \varepsilon_{11} + \varepsilon_{22} + \varepsilon_{33} \tag{4}$$

The constitutive equation in Eq. 5:

$$\sigma'_{ij} = \sigma_{ij} - \alpha p \delta_{ij} = \lambda \delta_{ij} \varepsilon_v + 2G\varepsilon_{ij} \tag{5}$$

The seepage equation in Eq. 6:

$$K\nabla^2 p = \frac{1}{Q}\frac{\partial p}{\partial t} - \alpha \frac{\partial \varepsilon_v}{\partial t} \tag{6}$$

where ρ is the density; σ_{ij} is the summation of normal stresses; ε_v, ε_{ii} are the volumetric strain and normal strain, respectively; δ is the Kronecker constant; Q is the Biot constant; G and λ are the shear modulus and the Lame constant, respectively; and ∇^2 is the Laplace operator.

The change of the permeability coefficient during the seepage-stress coupling is denoted in Eq. (7):

$$k(\sigma, p) = \xi k_0 \mathrm{e}^{-\beta\left(\frac{\sigma_{ii}}{3} - \alpha p\right)}, \tag{7}$$

where k_0 is the permeability coefficient, p is the pore water pressure, ξ is the mutation coefficient of permeability coefficient, α is the coefficient of pore water pressure, and β is the coupling coefficient (stress sensitivity factor) which is determined by experiments and varies under different stress states.

Furthermore, a large amount of experimental results indicated that the permeability coefficient is not only a function of stress, but also varies remarkably during the damage and failure evolution process induced by stresses. In RFPA-Flow, the variation of the permeability coefficient beyond the elastic behaviour of the rock is associated with the damage and failure process of the rock under various loading conditions. When the stress or strain state of an element satisfies a prescribed damage threshold, the element damage occurs. The elastic modulus of the damaged element is denoted by Eq. (8):

$$E = (1 - D)E_0, \tag{8}$$

where D is the damage variable; E and E_0 are the elastic modulus of the damaged and non-damaged elements. The

variation of the damage variable D depends on the failure type and the strain state of the element. Let us take an element under the uniaxial tensile stress as an example. When the element stress reaches the damage threshold, i.e. the tensile strength f_t in Eq. (9) in this case,

$$\sigma_3 \leq -f_t \tag{9}$$

the damage variable can be denoted using Eq. (10)

$$D = \begin{cases} 0, \varepsilon_{t0} \leq \varepsilon; \\ 1 - \dfrac{f_{tr}}{E_0 \varepsilon}, \varepsilon_{tu} \leq \varepsilon \leq \varepsilon_0; \\ 1, \varepsilon \leq \varepsilon_{tu}. \end{cases} \tag{10}$$

where f_{tr} is the residual strength; and ε_{t0} and ε_{tu} are the maximum tensile strain and ultimate tensile strain, respectively.

The corresponding permeability coefficient of the element follows Eq. (11):

$$K = \begin{cases} K_0 e^{-\beta(\sigma_3 - \alpha p)}, D = 0 \\ \xi K_0 e^{-\beta(\sigma_3 - \alpha p)}, 0 < D < 1 \\ \xi' K_0 e^{-\beta(\sigma_3 - p)}, D = 1. \end{cases} \tag{11}$$

Similarly, the equations denoting the variations of the damage variable and the permeability coefficient of the elements under uniaxial compression can be obtained during the element damage and failure process, as depicted in Fig. 1. Moreover, these equations can be extrapolated to denote the variations of the damage variable and the permeability coefficient of the elements under multi-axial loading conditions.
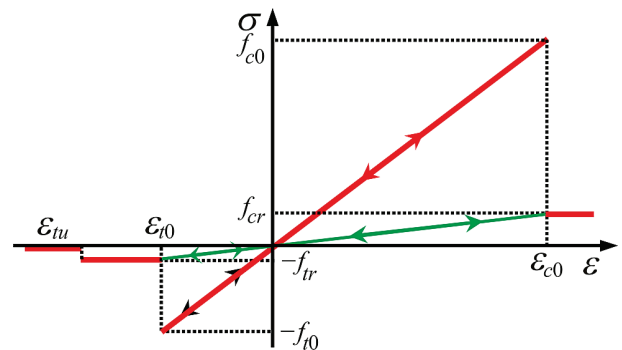

Figure 1 Constitutive model of mesoscopic element under uniaxial compression and tension

2.2 Criterion for hydraulic fracture propagation

The propagation and failure criterion is necessary in order to study extension of hydraulic fractures. The elastic energy dissipated for per unit of newly created fracture surface area is defined as the energy release rate for fracture propagation and denoted by G. The critical energy release rate is represented by G_c, which is a constant independent of external loading condition and geometric shape of fractures. For a system containing a single fracture with the fracture length of a, the fracture starts to propagate when $G = G_c$ and $dG/da > 0$.

Table 1 Testing results on the air permeability and fluid permeability of the propped fractures

No.	Length (10^{-2}m)	Sectional area (10^{-4}m²)	Porosity (%)	Confining pressure (10^6 Pa)	Gas permeability (m/d)	Artificial fracture retention fluid permeability (m/d)
2	5,06	4,745190	4,54	3	0,187300	6,835531
				5	-	3,417766
				10	-	0,746739
				15	-	0,165215
				20	-	0,047063
				25	-	0,023856
				30	-	0,018089
				35	-	0,017518
5	4,12	4,807170	3,5	3	0,901725	79,356807
				5	0,389048	27,469664
				10	0,201337	4,709085
				15	0,066633	1,414279
				20	0,035272	0,532993
				25	0,021305	0,222495
				30	0,006739	0,118870
				35	0,004738	0,062285
7	3,88	4,838307	2,11	3	0,005100	3,238241
				5	-	2,267683
				10	-	0,283911
				15	-	0,130231
				20	-	0,066217
				25	-	0,058815
				30	-	0,045093
				35	-	0,036302
8	3,808	4,861728	2,62	3	0,010081	150,305880
				5	0,002691	95,649196
				10	0,001607	41,486263
				15	0,000977	13,054344
				20	0,000156	6,943800
				25	0,000126	3,231273
				30	0,000104	1,773688
				35	0,000083	0,206621
9	4,592	4,799399	2,48	3	0,006900	4,622157
				5	-	1,854237
				10	-	0,512747
				15	-	0,204879
				20	-	0,074284
				25	-	0,040576
				30	-	0,022197
				35	-	0,013629
12	3,334	4,830513	3,76	3	0,055036	10,955489
				5	0,021160	5,638855
				10	0,011176	1,567914
				15	0,003916	0,595304
				20	0,002219	0,056932
				25	0,001701	0,050568
				30	0,000497	0,038770
				35	0,000395	0,031212

Therefore, G and dG/da need to be calculated accurately. For a system containing multiple fractures, the energy release rate at the ith crack tip can be obtained according to Eq. (12) by the finite element method.

$$G_i = -\frac{\partial \Pi}{\partial \alpha_i} = -\frac{1}{2} u^{\mathrm{T}} \frac{\partial K}{\partial \alpha_i} u + u^{\mathrm{T}} \frac{\partial f}{\partial \alpha_i}. \tag{12}$$

When $i \neq j$,

$$\frac{\partial G_i}{\partial \alpha_j} = -u^{\mathrm{T}} \frac{\partial K}{\partial \alpha_i} K^{-1} \left[\frac{\partial f}{\partial \alpha_i} - \frac{\partial K}{\partial \alpha_j} u \right] +$$
$$+ \left[\frac{\partial f}{\partial \alpha_j} - \frac{\partial K}{\partial \alpha_j} u \right] K^{-1\,\mathrm{T}} \frac{\partial f}{\partial \alpha_i}. \tag{13}$$

When $i = j$,

$$\frac{\partial G_i}{\partial \alpha_i} = -u^{\mathrm{T}} \frac{\partial K}{\partial \alpha_i} K^{-1} \left[\frac{\partial f}{\partial \alpha_j} - \frac{\partial K}{\partial \alpha_j} u \right] - \frac{1}{2} u^{\mathrm{T}} \frac{\partial^2 K}{\partial \alpha_i^2} u +$$

$$+ \left[\frac{\partial f}{\alpha \alpha_i} - \frac{\partial K}{\partial \alpha_i} u \right] K^{-1\mathrm{T}} \frac{\partial f}{\partial \alpha_i} + u^{\mathrm{T}} \frac{\partial^2 f}{\partial \alpha^2}. \tag{14}$$

where K is the stiffness matrix of the structure, f is the loading vector and u is the displacement vector.

Table 2 Testing results for Kaiser effects of the recovered rock core under confining stresses

Well No	Lithology	Core No.	Depth (m)	Specimen No.	Coring position	Geostress (10^6 Pa)	Horizontal maximum geostress (10^6 Pa)	Horizontal minimum geostress (10^6 Pa)	Vertical geostress (10^6 Pa)
Well 69 of Luojia area	Shale	$18\frac{13}{31}$	3050,2÷3052,2	1	Vertical direction	60,96	55,52	47,64	61,00
				2	0°	53,90			
				3	45°	48,40			
				4	90°	49,26			
		$18\frac{13}{31}$	3048,2÷3050,2	5	0°	52,27	55,48	47,56	60,23
				6	45°	47,66			
				7	90°	50,80			

Table 3 Results of uniaxial compressive tests on rock specimens

Well No.	Lithology	Core No.	Depth (m)	Specimen No.	Diameter D (10^{-3}m)	Height H (10^{-3}m)	Uniaxial compressive strength σ_1 (10^6 Pa)	Elastic Modulus E (10^{10} Pa)	Poisson's ratio ν
Well 69 of Luojia area	Shale	$18\frac{4}{31}$	3048,2÷3050,2	A3	24,96	48,56	28,288	1,539	0,156
				A4	24,54	49,20	72,010	2,576	0,125
		$18\frac{4}{31}$	3046,2÷3048,2	C1	24,60	49,80	39,281	1,583	0,305
				C2	24,52	47,60	53,794	1,992	0,293
-	-	-	-	Mean value	-	-	48,34	1,923	0,220

2.3 Determination of parameters by physical tests

In this study, a well drilled by Sinopec Corp. in Luojia area of Shengli Oilfield is considered. The strata in the well region from top to bottom include: Pingyuan Group, Minghuazhen, Guantao Group, Dongying Group, Shahejia Group (from Shahejie Section One to Shahejie Section Four). The total well depth is 3390 m, and the depth below the technical casing is 2907,68 m. The well section has a diameter of 311,10 mm and a length of 2910 m. In order to overcome the challenges brought by large stratum dipping angle, tilting strata and multiple interbed, the techniques, such as vibration reduction and pressurization, and optimized drill bits, were adopted to improve the drilling speed at large well sections. The records at that area indicate that high technical indicators have ever been achieved in similar fields. After the third spud, 200 m long continuous sealed core was drilled in corporation with Drilling Technology Research Institute. In spite of the lack of knowledge on strata and lithology, large depth of coring location, hard and compact rock, poor drillability and water inflow, 229,75 m core was successfully recovered, with the recovery rate being 96 %. The recovered core can be used to better understand gas storage in the shale gas reservoir at the Lower Shahejie Section Three of the Luojia area.

The mechanical tests on the rock specimens collected from the shale gas reservoir bed and relevant physical model tests on fracture initiation and propagation serve as the basis for the following numerical analysis. Tests on the permeability of the propped fractures were also conducted and the relevant results are listed in Tab. 1. The testing results on the Kaiser effect of the rock specimens

under confining stresses are listed in Tab. 2. As can be seen from Tab. 2, the maximum horizontal stress is 55MPa. The results of the uniaxial compressive tests of the rock specimens are listed in Tab. 3.
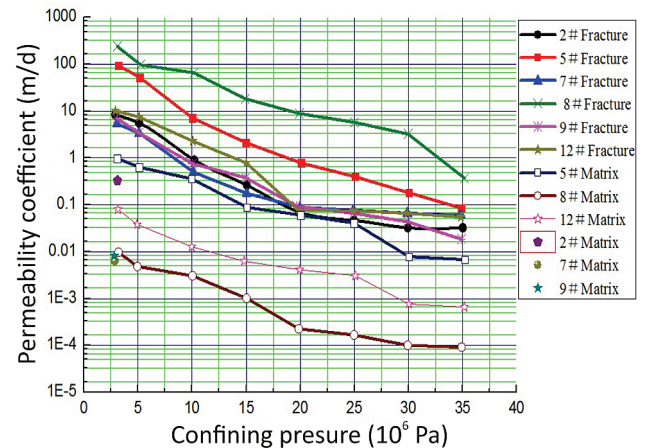
Figure 2 Relationship between confining stress and permeability

The testing results indicate that the matrix permeability of shale specimens varies in a wide range. As shown in Fig. 2, under a confining stress of 3 MPa, the maximum matrix permeability is 0,9 m/d, while the minimum is only 0,0051 m/d. Meanwhile, the matrix permeability of the shale is significantly affected by the confining stresses. The matrix permeability is increased by about 50 % in average with an increment of 5 MPa for the confining stress. The analysis results reveal that the difference can be attributed to sedimentary stratification. The effect of the confining stress on the matrix

permeability is less significant if less sedimentary stratifications are present. If there are a number of sedimentary beds, the degree of the strata closure increases, leading to a significant reduction of the matrix permeability. In this study, the porosity of the shale specimen is very low under atmospheric pressure, roughly between $2 \div 5$ %. In order to investigate the enhancement effect of unfilled fracture on the permeability of shale, in situ permeability tests were carried out after artificial fractures were closed.

As can be seen from the testing results, although some unfilled or dislocated fractures were closed, the systematic permeability of propped fractures was enhanced substantially. The matrix permeability was increased by $1 \div 4$ order of magnitude, and, in average, 3 order of magnitude. Therefore, hydraulic fracturing is worthy of being performed in that area for more efficient exploitation of the shale gas reservoir. The experimental data indicated that the permeability was increased by about 3 order of magnitude even if the fractures were unfilled, which is significant for the efficient exploitation of shale gas in that area. Based on the above physical testing results, the physical and mechanical parameters of the shale are summarized in Tab. 4.

Table 4 Parameters of the various layers of the horizontal well for the numerical modelling

| Mechanics and control parameters	Calcite (70%)	Quartz (10%)	Clay (20%)	Overall
Homogeneous degree m	2	2	2	2
Average elastic modulus E_0 (10^9 Pa)	33,9	56,5	11,3	33
Average compressive strength σ_0 (10^9 Pa)	1440	2400	480	220
Friction angle φ(°)	45	45	45	45
Ratio of compressive strength and tensile strength C/T	15	15	15	15
Poisson's ratio μ	0,26	0,26	0,26	0,26
Cohesion (10^9 Pa)	2,54	2,54	2,54	2,54
Residual strength coefficient ξ	0,1	0,1	0,1	0,1
Permeability k (m/d)	$0,01 \div 1$	$0,01 \div 1$	$0,01 \div 1$	$0,01 \div 1$
Permeability coefficient K (m/d)	$8,64 \times 10^{-5}$	$4,32 \times 10^{-5}$	$4,32 \times 10^{-4}$	$0,864 \times 10^{-3}$

3 Effect of the ratio between vertical stress and maximum horizontal stress on the initiation and propagation of hydraulic fractures

Geostresses are the fundamental data for the development scheme of oilfield, the analysis of the propagation law of hydraulic fractures, and the prediction of stratum breakdown and fracturing stress. The differences between the physical and mechanical properties of various rock types in or between strata and these between the pore water pressures in the strata may lead to heterogeneous geostress distribution in or between strata. Moreover, the geostress plays a significant role in determining the hydraulic fracture initiation pressure, fracture initiation location, fracture propagation, and fracture pattern. Thus, the geostress is an important factor for fracture propagation during hydraulic fracturing. In this section, the effect of the difference between the vertical stress and the maximum horizontal stress on the propagation mechanism and law of hydraulic fractures will be discussed.
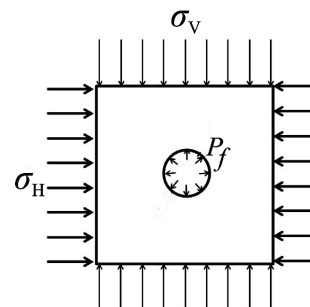
3.1 Numerical models

In this section, the seepage module of the realistic failure process analysis software (RFPA-FLOW) is adopted to simulate the effect of the difference between the vertical stress and the maximum horizontal stress on the initiation and propagation of hydraulic fractures. A two-dimensional rectangular model was built as shown in Fig. 3. The model has a dimension of 1200×1200 mm and consists of $600 \times 600 = 360\,000$ elements. The loading condition is shown in Fig. 4. The model boundaries are impervious. A well with a diameter of 139 mm is created in the centre of the model. To model hydraulic fracturing, a gradually increasing hydraulic pressure P_f is applied in the wellbore. The initial hydraulic pressure is 23 MPa and the hydraulic pressure is increased with an increment of 1 MPa per step until fractures are initiated and propagate leading to the specimen failure. A steady-state seepage field is assumed throughout the simulation. In order to investigate the effect of the difference between the vertical stress and the maximum horizontal stress on hydraulic fracture propagation, various combinations of the vertical stress and the maximum horizontal principal stress are selected, as shown in Tab. 5. The ratio of the vertical stress and maximum horizontal principal stress is defined as λ. Six modelling schemes are designed, in which the vertical stress remains unchanged (constant σ_V) and the maximum horizontal principal stress is increased gradually (increasing σ_H).
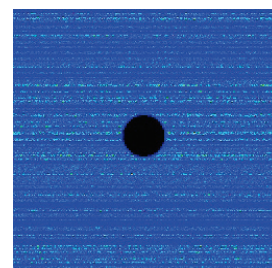
Figure 3 Numerical model for the stratified rock mass with a horizontal well

Figure 4 Schematic sketch of the loading conditions for the numerical model

Table 5 Schemes of numerical tests

| Scheme	1	2	3	4	5	6
σ_V (10^6 Pa)	61	61	61	61	61	61
σ_H (10^6 Pa)	61	55	51	47	41	31
Stress ratio, λ	1	1,1	1,2	1,3	1,5	2

The fundamental mechanical parameters of the rock material, such as elastic modulus, Poisson's ratio, compressive to tensile strength ratio and friction angle, are taken from Tab. 4. The homogeneity index of the model is assumed as 2 so as to reflect the mesoscopic heterogeneity of the rock material. The strength, elastic modulus, Poisson's ratio and other parameters are assumed to satisfy the Weibull distribution aforementioned.
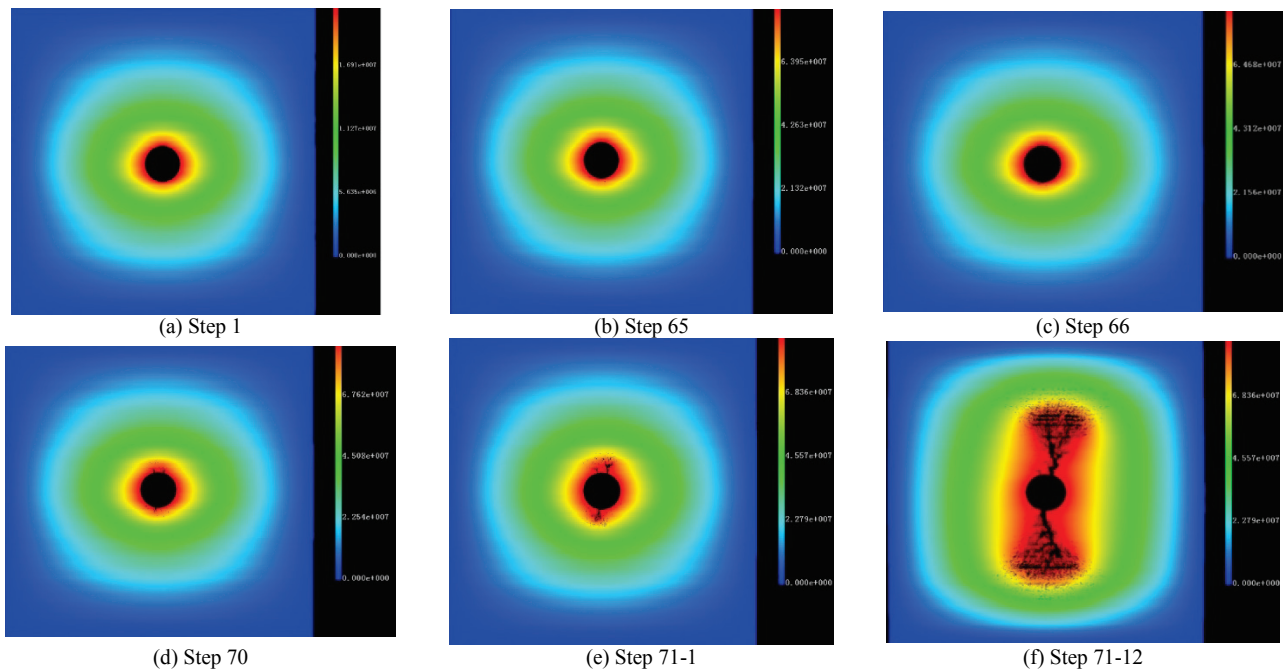
3.2 Modelling results and analyses

(1) Scheme 2 (σ_V = 61 MPa, σ_H =55 MPa, λ = 1,1)

Figs. 5, 6 and 7 present the distribution of the modelled minimum principal stress, pore water pressure, and acoustic emission, respectively, in the rock with the in-situ stresses of σ_V = 61 MPa and σ_H = 55 MPa as the hydraulic pressure in the well increases. According to the numerical simulation, the rock fracture process during the hydraulic fracturing can be divided into three stages, i.e., pre-fracturing, microfracturing and fracturing stages.

(a) Step 1	(b) Step 65	(c) Step 66
(d) Step 70	(e) Step 71-1	(f) Step 71-12
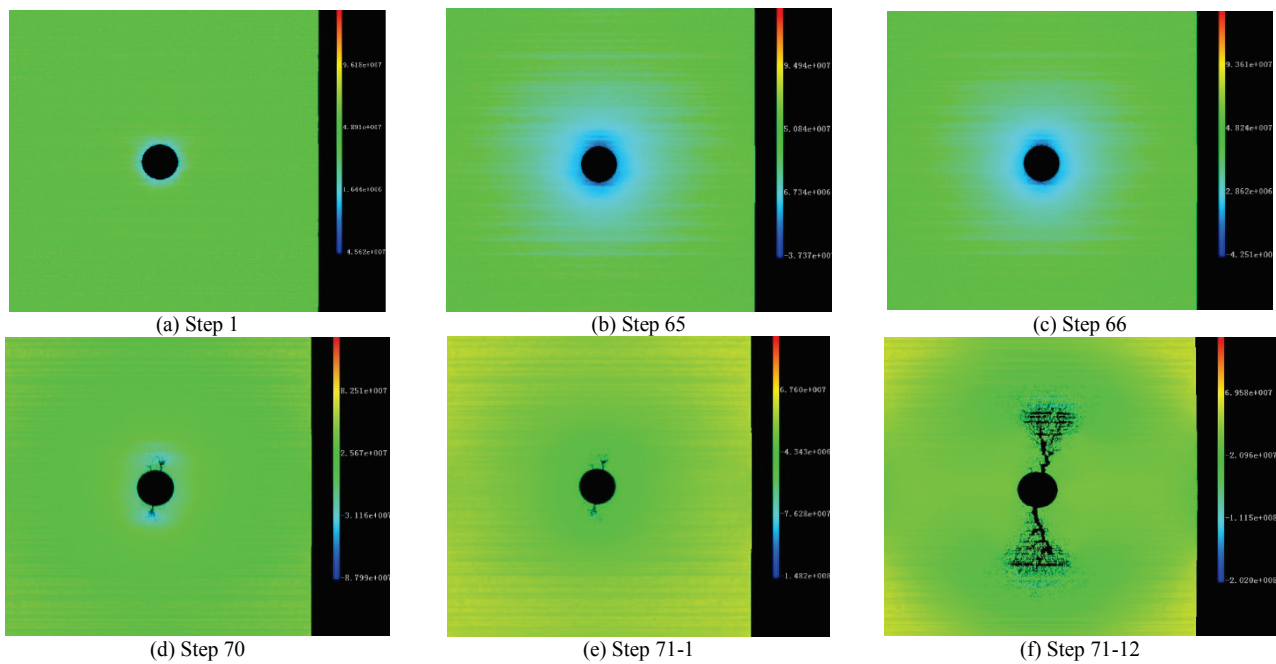
Figure 5 Distribution of minimum principal stress for Scheme 2 (λ = 1,1, unit: Pa)

(a) Step 1	(b) Step 65	(c) Step 66
(d) Step 70	(e) Step 71-1	(f) Step 71-12

Figure 6 Distribution of pore water pressure for Scheme 2 (λ = 1,1, unit: Pa)

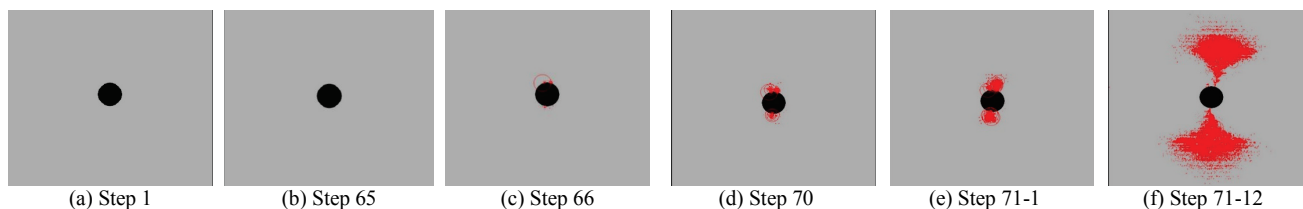| (a) Step 1 | (b) Step 65 | (c) Step 66 | (d) Step 70 | (e) Step 71-1 | (f) Step 71-12 |

Figure 7 Plot of acoustic emissions for Scheme 2 ($\lambda = 1,1$)

The pre-fracturing stage includes Step 1 ÷ Step 65, in which the hydraulic pressure increases from 23 MPa to 85 MPa. During this stage, the specimen remains elastic and no element damage or failure occurs in the model. However, the stress continuously accumulates and concentrates in this stage, especially at the upper and lower boundaries of the well. Since the horizontal stratification is considered, stratified distribution of high stresses can be observed in the rock surrounding the well. The pore water pressure is distributed symmetrically in an elliptical shape with its centre at the centre of the well (Figs. 6a and 6b). The pore water pressure decreases exponentially from the well wall to the model boundary. Almost no acoustic emissions are recorded in Figs. 7a and 7b, which is consistent with the result obtained by laboratory tests.

The fracture initiation and propagation stage includes Step 66 ÷ Step 70, in which the hydraulic pressure is between 86 MPa and 90 MPa. In this stage, with the further increase of the hydraulic pressure in the well, high stresses are accumulated at the well wall to a certain extent. At some locations with low strengths or high stresses, the tensile strength of the rock medium is satisfied leading to the occurrence of elemental damage. The red circles in Fig. 7c represent tensile stress - induced acoustic emissions, indicating that the failure mode is dominantly tensile failure. In Fig. 7d, a few white circles appear, too, showing that the acoustic emissions are caused by the elemental shear damages induced by shear stresses. It can be seen from Fig. 7, initially, the damaged elements are scattered. With increasing number of the damaged elements, these elements gradually cluster and microfractures are initiated. With further increasing of the hydraulic pressure, the microfractures propagate approximately along the vertical direction. It is also noticed that sporadic microfractures, which are not connected to the main fracture, appear near the fracture tip. The fracturing and failure stage includes Step 71, in which the hydraulic pressure reaches 91 MPa. As the hydraulic pressure keeps increasing, the microfractures coalesce to form a main fracture, which propagates in non-linear paths. It is noted that the fractures are curved or branched at some locations. Moreover, multi-layered fractures also occur, which is mainly caused by dominant tensile failures due to the effect of stratification. The formed macroscopic fracture propagates approximately in the vertical direction. With increasing number of the damaged elements in the vicinity of the formed macroscopic fracture, the tip of the fracture moves forward and the fluid with the high pressure flows into the fracture tip leading to high stresses there. Thus, the high stress zone is shifted to the crack tip and the high stress there becomes the driving force for further fracturing. As can be seen from Figs. 5e and 5f, the size, length and propagation direction of the fractures formed around the upper and lower boundaries of the well are not exactly the same, which is caused by the heterogeneity of the rock material.

Table 6 Final fracture pattern for various stress combinations (plots of pore water pressure and acoustic emission)

λ	1	1,1	1,2	1,3	1,5	2,0
Distribution of pore water pressure						
Plot of acoustic emissions						

The final fracture pattern is basically an approximately symmetrical double-wing crack. From the acoustic emissions in Figs. 7e and 7f, it can be seen that the main failure mode is tensile failure, which is indicated by the red color, and the final fracture pattern is fan-shaped. The simulation results well explain why tensile failure is dominant during hydraulic fracturing in stratified shale. As long as the hydraulic pressure is high enough, the rock at very far distance can be fractured. However, given that the ratio of vertical stress and

maximum horizontal principal stress is 1,1, which is relatively small, a large area of microfractures can be formed instead of narrow and long hydraulic fractures, which is usually accompanied with the higher stress ratio.

As can be seen from the numerical simulation above, the rock deformation and failure process under hydraulic fracturing is a gradual deterioration process. With increasing hydraulic pressure in the well, microfractures or micro-holes have been formed in most hydraulically fractured rock mass before the occurrence of macroscopic fracture. Under the effect of various external factors, the microfractures and micro-holes are continuously initiated, propagate, coalesce and connect with each other. The physical-mechanical properties of the hydraulically fractured rock mass are deteriorated. As a result, the strength, stiffness and toughness of the rock mass are degraded. This process is called the damage process of the rock mass under hydraulic fracturing. During the entire process, due to the existence and evolution of the rock mass damage, the hydraulically fractured rock masses become further heterogeneous and discontinuous. Thus, the hydraulic fracturing process is in fact a process from initiation, propagation and coalescence of microfractures to formation of macrofractures and a process of increasing rock mass heterogeneity and discontinuity.

(2) Other modelling schemes

Tab. 6 summarizes the final fracture patterns and the corresponding acoustic emissions of the rock mass under different stress combinations during hydraulic fracturing. As can be seen from Tab. 6, only when the ratio between the vertical stress and the maximum horizontal principal stress is 1, the hydraulic fractures develop along the horizontal direction.

The fracture propagation direction is perpendicular to the horizontal stratifications in all other cases, i.e., along the direction of the vertical stress but the fracture pattern and length are different for different stress combinations, which are discussed in the following paragraphs.
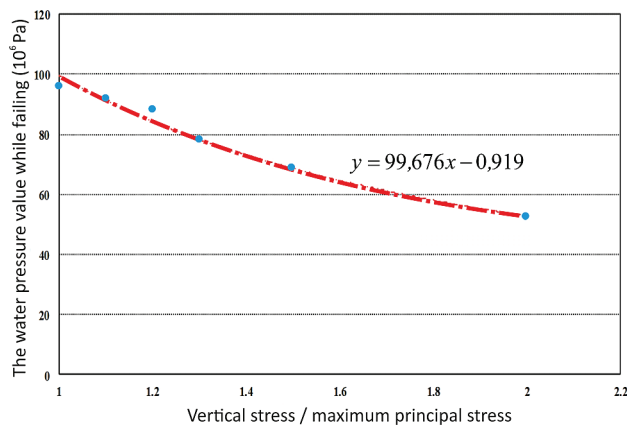
Figure 8 Relationship between the break-down hydraulic pressure and the in-situ stress ratio

1) When the confining stresses are high, failure occurs suddenly in the rock mass without the formation of large damaged area and with few acoustic emissions after the hydraulic pressure reaches a certain value.

2) Branched fractures are likely to form in stratified rock masses under hydraulic fracturing. The branch fractures occur at a distance of approximately 5 times of the perforation length.

3) When the ratio between the vertical stress and maximum horizontal principal stress is 1, the effect of the stratification is most obvious and the hydraulic fractures propagate along the horizontal stratification direction. When the ratio is between 1 and 1,5, the hydraulic fractures propagate perpendicularly to the stratification direction. However, the fracture propagation is affected by the stratification and more branch fractures are likely to occur along the stratification. When the ratio is greater than 1,5, the hydraulic fractures are less affected by the stratifications and less branch fractures are formed compared with those in the case that the ratio is between 1 and 1,5. Moreover, it is found that longer hydraulic fractures are formed even under lower hydraulic pressures when the ratio becomes bigger.

4) Fig. 8 depicts the relationship between the breakdown pressure, i.e. the hydraulic pressure when failures occur, and between the vertical stress and the maximum horizontal principal stress. It can be seen from Fig. 8 that the breakdown pressure decreases non-linearly with the ratio increasing. The break-down pressure is 96 MPa when the ratio is 1, which is about twice of that (52 MPa) when the ratio is 2.

4 Effect of the perforation angle on the initiation and propagation of hydraulic pressures

At present, almost all wells are completed by perforation. Therefore, hydraulic fracturing is usually performed in the perforated well. The perforation is a channel between the well and rock strata. Fluid is pumped into the rock strata through the perforations. Therefore, the parameters of the perforations inevitably affect the hydraulic fracturing process. Proper parameters of the perforations can be determined based on the previous studies by experts and the analyses by site engineers, so as to reduce the fracture initiation pressure, reduce the degree of fracture distortion and avoid multiple fractures. The auxiliary directional hydraulic perforation technique has been successfully applied in oilfields worldwide. However, it has seldom been reported how to reduce the fracturing pressure and enhance the fracturing efficiency by adjusting the perforation angle.

In this section, a series of numerical simulations is conducted to study how the perforation parameters affect the hydraulic fracturing in wellbores completed by perforation and how the perforation orientation influences the hydraulic fracture initiation and propagation. Based on the numerical simulation results, the effect of the directional perforation angle on the fracture initiation, propagation and pattern is discussed.
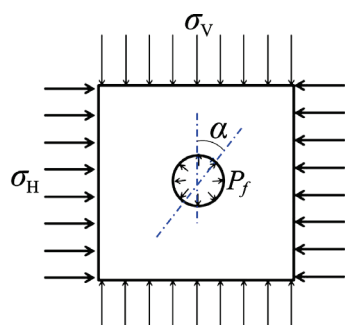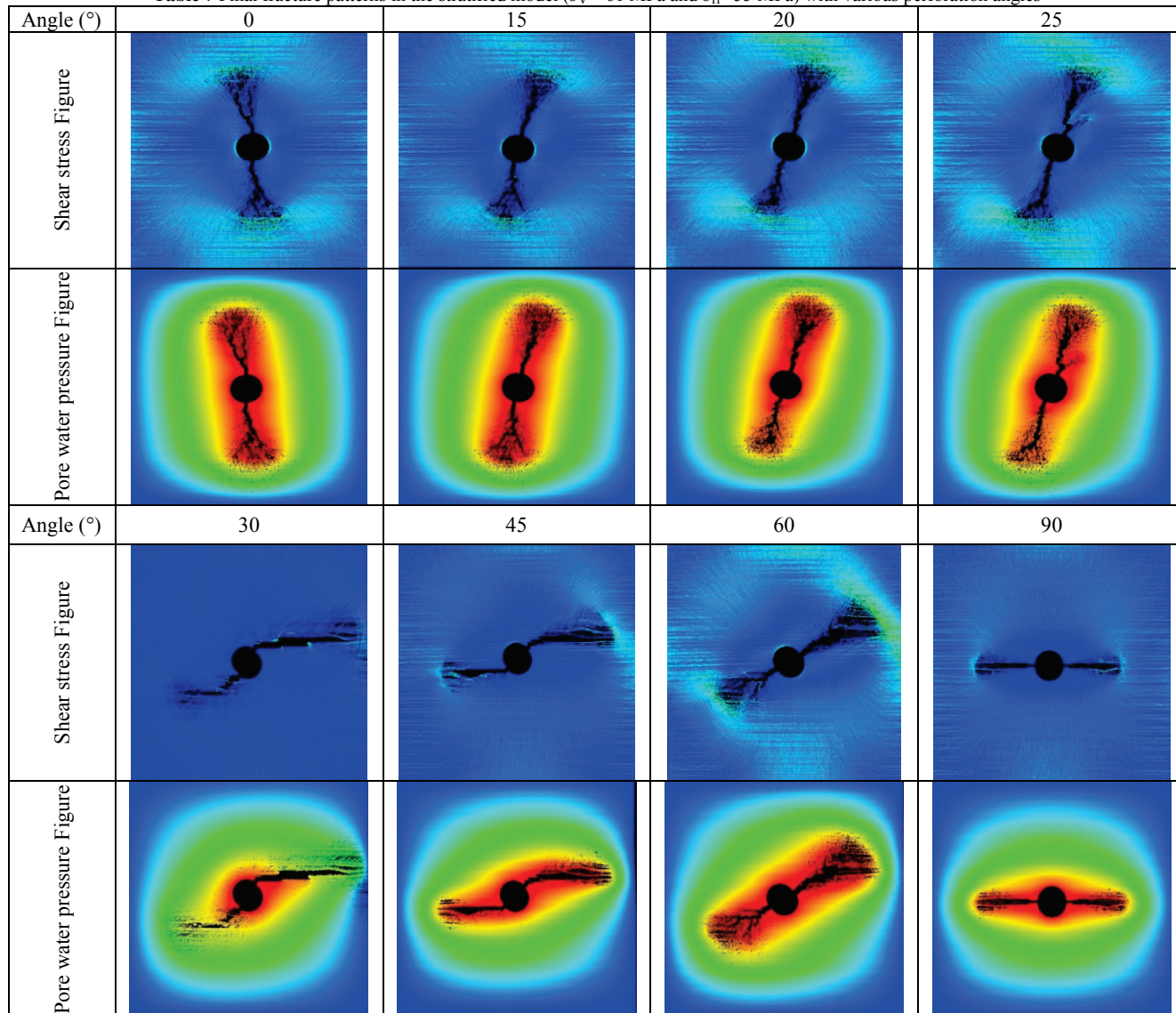
4.1 Numerical models

In this section, a two-dimensional rectangular model is designed to simulate the hydraulic fracturing in a stratified rock mass medium through a horizontal well with different perforation angles, as shown in Fig. 9. The model size is 1200 × 1200 mm, consisting of 600 × 600 = 360 000 elements. A wellbore is created in the model centre. An increasing hydraulic pressure P_f is applied in

the wellbore. The four boundaries of the model are impervious. The initial hydraulic pressure of the wellbore is set as 23 MPa, which is then increased by 1 MPa per step until the fractures propagate and the rock mass medium fails. Steady-state seepage is assumed again throughout the simulation. In the numerical simulation model, the angle between the perforation direction and the vertical principal stress direction is α, and the perforation length is 20 mm. The physical-mechanical parameters of the rock material, including elastic modulus, Poisson's ratio, compressive to tensile strength ratio and friction angle, are listed in Tab. 4.

Table 7 Final fracture patterns in the stratified model (σ_V = 61 MPa and σ_H =55 MPa) with various perforation angles

Angle (°)	0	15	20	25
Shear stress Figure				
Pore water pressure Figure				
Angle (°)	30	45	60	90
Shear stress Figure				
Pore water pressure Figure				

Figure 9 Schematic sketch of the numerical model

The homogeneity index is assumed to be 2 in order to reflect the mesoscopic heterogeneity of the rock material. The strength, elastic modulus and Poisson's ratio are assumed to satisfy the Weibull distribution in Eq. (1). Five cases with the perforation angles of 90°, 60°, 45°,

30° and 0° are simulated to investigate the effect of the perforation angle on the hydraulic fracturing in the stratified rock mass with the in-situ stresses of σ_V = 61 MPa and σ_H = 55 MPa.

4.2 Modelling results and analyses

Tab. 7 summarizes the final fracture patterns caused by the hydraulic fracturing in the stratified models under the in-situ stresses of (σ_V = 61 MPa and σ_H = 55 MPa) for the five cases. It can be seen from Tab. 7, for the stratified rock mass under such stress combination, if the perforation angle is greater than 30°, the hydraulic fractures are mainly affected by the stratifications. Hydraulic fractures are initiated at the tips of the perforation, then turn to the nearest stratification and finally propagate along the horizontal stratification.

Meanwhile, multiple parallel fractures are formed at the tips of the hydraulic fractures due to the stress concentration at the tips of the fractures. If the perforation angle is less than 30°, the hydraulic fractures are still initiated at the tips of the perforation but more branched fractures occur. Finally, the hydraulic fractures propagate approximately in the vertical direction.

Table 8 Final fracture pattern of the rock mass model under different stress ratios (σ_V/σ_H) and with different perforation angles
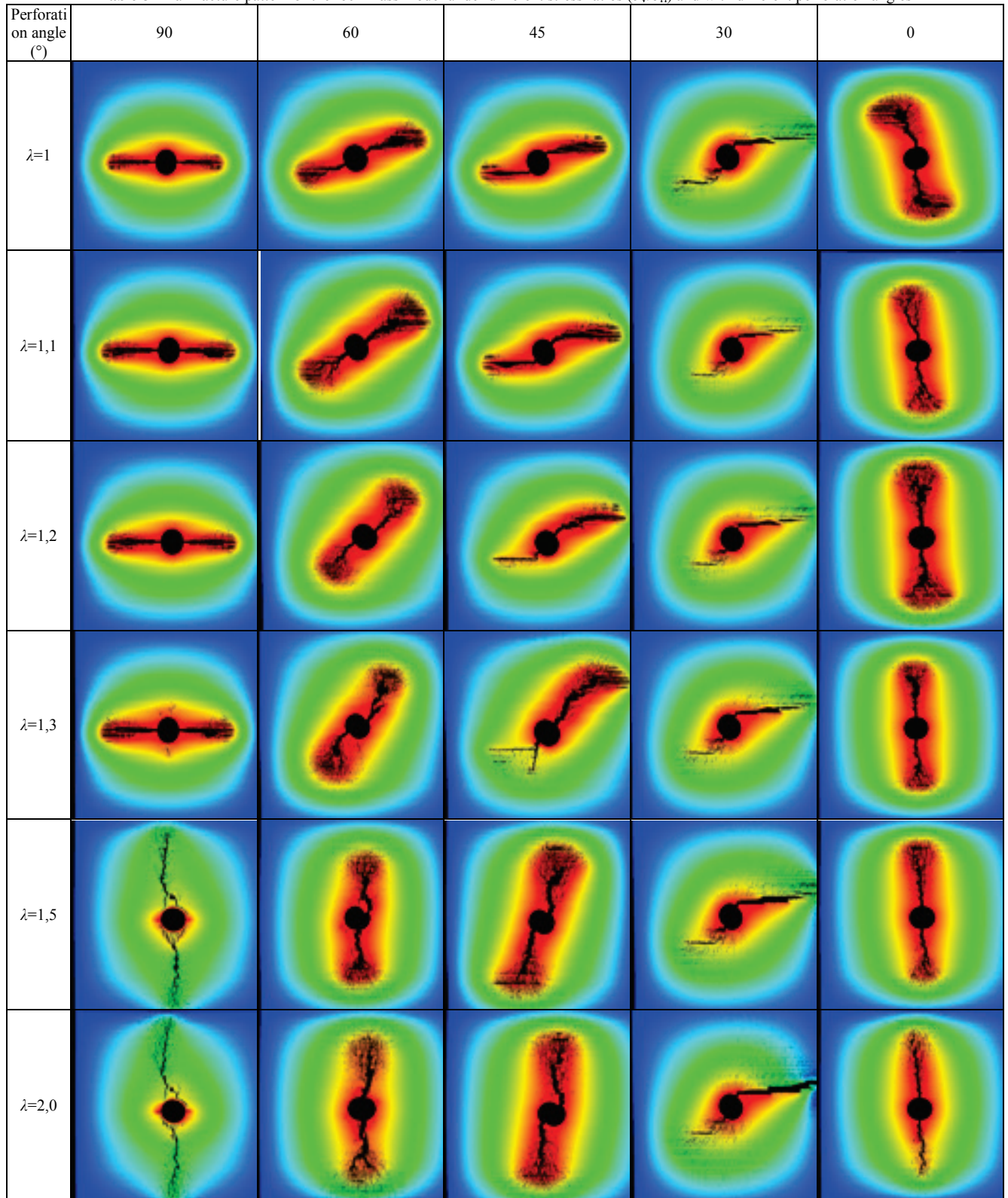
Besides studying the effect of the perforation angle on the hydraulic fracturing, the stress ratios (σ_V/σ_H) are also varied to study their effect on the hydraulic fracturing in the stratified rock mass with a certain perforation angle.

The corresponding results are shown in Tab. 8 and Fig. 10. As shown in Fig. 10, under the same stress ratio, the hydraulic pressure required for the complete fracturing of the rock mass medium with a perforation angle of 30° is

higher than all other cases. If the perforation angle is the same, the hydraulic pressure required for the complete fracturing of the rock mass medium increases with the stress ratio decreasing. Moreover, from the analysis of the specific shape of the cracks, it can be concluded that, when the perforation direction is perpendicular to the vertical principal stress, no fractures are initiated from the perforation when the stress ratio between the vertical stress and the maximum horizontal principal stress is greater than 1,3. Instead, the fractures are initiated along the vertical direction. As a result, the casing is stripped away and a ring fracture surrounding the casing is formed. In all other cases, the hydraulic fractures are initiated from the tips of the perforation and propagate along the stratification direction. Compared with the case without the stratification, a higher stress difference is required to form the ring fractures due to the effect of the stratification. Due to the effects of the stratification and high stress difference, the hydraulic fractures are formed at the tips of the perforation and then turn to propagate along the stratification direction in the model with the perforation angles of 30° and 45°. For the model with a perforation angle of 0°, the larger the ratio between the vertical stress and the maximum horizontal principal stress, the narrower and longer the hydraulic fractures and the less the branch. Moreover, the following summary can be made.
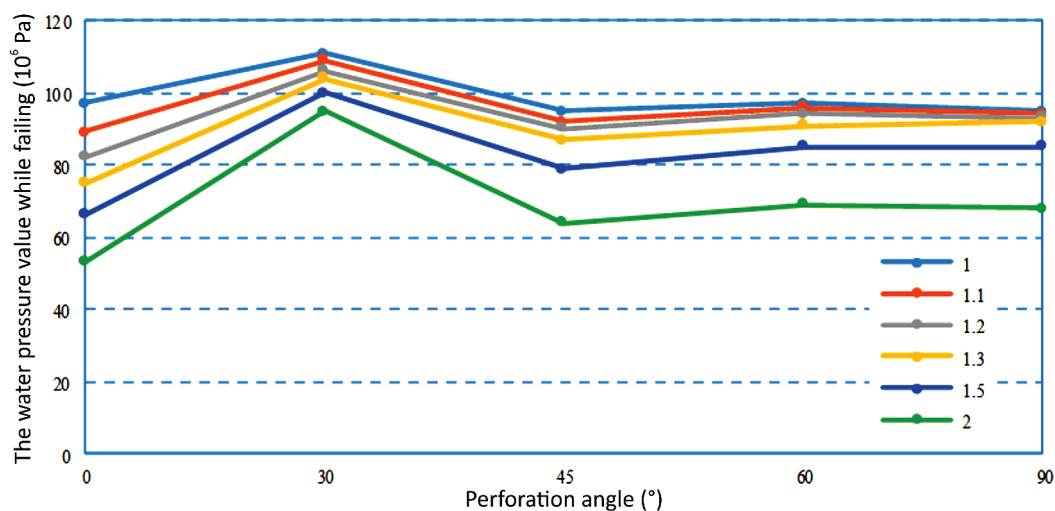

Figure 10 Plot of hydraulic pressures upon failure for different stress ratios and perforation angles

1) For the rock mass medium with the same perforation angle, the larger the stress ratio (i.e., lower maximum horizontal principal stress when the vertical stress remains constant), the lower the hydraulic pressure required for its complete hydraulic fracturing, i.e., the easier the hydraulic fracture formed.

2) For the rock mass medium under the same stress ratio, the hydraulic pressure required for its complete fracturing is higher in the case with a perforation angle of 30° than all other cases.

3) When the perforation direction is perpendicular to the vertical principal stress, no fractures are initiated from the perforation if the stress ratio between the vertical stress and the maximum horizontal principal stress is greater than 1,3. Instead, the fractures are initiated in the vertical direction. As a result, the casing is stripped away and a ring fracture surrounding the casing is formed. In all other cases, the hydraulic fractures are initiated from the tips of the perforation and propagate along the stratification direction. Compared with the case without the stratification, a higher stress difference is required to form ring fractures due to the effect of the stratification.

4) Due to the effects of the stratification and high stress difference, the hydraulic fractures are formed at the tips of the perforation and then turn to propagate along the stratification direction in the rock mass model with the perforation angles of 30° and 45°. For the model with a perforation angle of 0°, the larger the ratio between the vertical stress and the maximum horizontal principal

stress, the narrower and longer the hydraulic fractures and the less the branch fractures. The smaller the stress ratio, the more pronounced the effect of the stratification, the more the branch fractures and the shorter the main fracture.

5) When the ratio between the vertical stress and the maximum horizontal principal stress is larger than 1,3 and the perforation angle is greater than 60°, the hydraulic fractures are completely controlled by the vertical stress.

5   Conclusion

A total of six different in-situ stress ratios and eight different perforation angles were considered for the hydraulic fracturing in the stratified rock mass. The obtained results from these various combinations indicate that, for the stratified rock mass with the same perforation angle, the larger the stress ratio (i.e., lower maximum horizontal principal stress when the vertical stress remains constant), the lower the hydraulic pressure required for its complete hydraulic fracturing, i.e. the easier the hydraulic fractures formed. Moreover, it is found that, for the stratified rock mass under the same stress ratio, the hydraulic fracturing pressure in the case of the horizontal well with a perforation angle of 30° is higher than that in all other cases. Furthermore, it is noted that the effect of the stratification becomes weaker with the stress ratio increasing.

Future research should be carried out to build three-dimensional (3D) models for the hydraulic fracturing in the stratified rock mass using the horizontal wells since the fluid that flows along the third direction may play a very important role in the process of the hydraulic fracturing. It is expected that the 3D models should be more convincing than the two-dimensional ones in terms of simulating the hydraulic fracturing. Moreover, the forming process of the 3D fracture network during the hydraulic fracturing stimulation in the shale gas reservoir can be simulated using the 3D models. As a result, a better comparison between the numerical simulation and the monitoring data from practical projects can be carried out, which is of great directive significance to engineering practice.

Acknowledgements

6   References

[1] Scott, K. Modern Shale Gas -Development in the United States: A Primer. // U. S. Department of Energy, Office of Fossil Energy, National Energy Technology Laboratory, 2002.

[2] Jiang, H. Y.; Song, X. M.; An, X. X. The review on world shale gas resources and exploration technology. // Natural Gas Technology. 2, 6(2008), pp. 26-30.

[3] Bai, Z. H.; Shi, B. H.; Zuo, X. M. The Study on Shale gas and its accumulation mechanism. // Natural Gas and Oil. 29, 3(2011), pp. 54-57

[4] Jia, L. C.; Chen, M.; Jin, Y. Progress of hydraulic fracturing fracture monitoring technology for shale gas wells in foreign countries. // Natural Gas and Oil. 30, 1(2012), pp. 44-47.

[5] Hubbert, M. K.; Willis, D. G. Mechanics of hydraulic fracturing. // Transaction of American Institute of Mining, Metallurgical, and Petroleum Engineers. 1972, pp.239-257.

[6] Sun, K. M.; Cui, H.; Lee, C. Q. Numerical simulation of propagation of oriented crack prefabricated in hydraulic fracturing. // Journal of Liaoning Technical University. 25, 2(2006), pp. 176-179.

[7] Zhao, J. J.; Ren, L.; Hu, Y. Q. Controlling factors of hydraulic fractures extending into network in shale formations. // Journal of Southwest Petroleum University (Science & Technology Edition. 35, 1(2013), pp. 1-9.

[8] Chen, M.; Pang, F.; Jin, Y. Experiments and analysis on hydraulic fracturing by a large-size triaxial simulator. // Chinese Journal of Rock Mechanics and Engineering. 19, (2000), pp. 868-872.

[9] Warpinski, N. R; Teufel, L. W. Influence of geologic discontinuities on hydraulic fracture propagation. //Journal of Petroleum Technology. 39, 2(1987), pp. 209-220. DOI: 10.2118/13224-PA

[10] Warpinski, N. R. Hydraulic fracturing in tight, fissured Media. // Journal of Petroleum Technology. 43, 2(1991), pp. 146-209. DOI: 10.2118/20154-PA

[11] Warpinski, N. R.; Lorenz, J. C.; Branagan, P.T. et al. Examination of a cored hydraulic fracture in a deep gas well. // Society of Petroleum Engineers Production & Facilities. 8, 3(1993), pp. 150-158. DOI: 10.2118/22876-PA

[12] Blanton, T. L. An experimental study of interaction between hydraulically induced and pre-existing fractures. // Society of Petroleum Engineers Unconventional Gas Recovery Symposium / Pittsburgh, 1982, pp. 559-571.

[13] Blanton, T. L. Propagation of hydraulically and dynamically induced fractures in naturally fractured reservoirs. // Society of Petroleum Engineers Unconventional Gas Technology Symposium / Louisville, 1986, pp. 613-627.

[14] Chen, M.; Pang, F.; Jin, Y. Experiments and analysis on hydraulic fracturing by a large size triaxial simulation. // Chinese Journal of Rock Mechanics and Engineering. 19(Sup.) (2000), pp. 868-872.

[15] Zhou, J.; Chen, M.; Jin, Y. et al. Experimental study on propagation mechanism of hydraulic fracture in naturally fractured reservoir. // Acta Petrolei Sinica. 5, 28(2007), pp. 109-113.

[16] Zhou, J.; Chen, M.; Jin, Y. et al. Experiment of propagation mechanism of hydraulic fracture in multi-fracture reservoir. // Journal of China University of Petroleum: Natural Science Edition. 4, 32(2008), pp. 51-54.

[17] Chen, M.; Zhou, J.; Jin, Y. et al. Experimental study on fracturing features in naturally fractured reservoir. // Acta Petrolei Sinica, 3, 29(2008), pp. 431-434.

[18] Mahrer, K. D. A review and perspective on far-field hydraulic fracture geometry studies. // Journal of Petroleum Science and Engineering. 24, 1(1999), pp. 13-28. DOI: 10.1016/S0920-4105(99)00020-0

[19] Beugelsdijk, L. J. L.; de, Pater, C. J.; Sato, K. Experimental hydraulic fracture propagation in multi-fractured medium. // Society of Petroleum Engineers Asia Pacific Conference on Integrated Modelling for Asset Management / Yokohama, 2000, pp. 101-108.

[20] Fisher, M. K.; Wright, C. A.; Davidson, B. M. et al. Integrating fracture mapping technologies to optimize stimulations in the Barnett shale. // Society of Petroleum Engineers Annual Technical Conference and Exhibition / San Antonio, 2002, pp. 230-236.

[21] Fisher, M. K.; Heinze, J. R.; Harris, C. D. et al. Optimizing horizontal completion techniques in the Barnett shale using microseismic fracture mapping. // Society of Petroleum Engineers Annual Technical Conference and Exhibition / Houston, 2004, pp.123-133.

[22] Maxwell, S. C.; Urbancic, T. I.; Zinno, R. Microseismic imaging of hydraulic fracture complexity in the Barnett shale. // Society of Petroleum Engineers Annual Technical Conference and Exhibition / San Antonio, 2002, pp. 25-33.

[23] Urbancic, T. I.; Maxwell, S. C. Microseismic imaging of fracture behavior in naturally fractured reservoirs. // SPE/ISRM Rock Mechanics Conference / Irving, 2002, pp. 152-158.

[24] Johannes, D. B; Lars, O. N. Process Simulation and Plant Layout of a Combined Cycle Gas Turbine for Offshore Oil and Gas Installations. // Journal of Power Technologies. 95, 1(2015), pp. 40-47.

[25] De Miguel, J. A.; Gutyrya, S. S.; Jomyak, Y. M. Stress in hollow axis with a surface crack under rotation and bending. // DYNA, 89, 1(2014), pp. 85-88.

Authors' addresses

Tianhui Ma, Ph.D. (Corresponding author)
State Key Laboratory of Coastal and Offshore Engineering, Dalian University of Technology
School of Civil Engineering, Dalian University of Technology
No. 2 Linggong Road, 116024 Dalian, P. R. China
E-mail: tianhuima@dlut.edu.cn

Quan-ao Wu, M.D Candidate
School of Civil Engineering, Dalian University of Technology
No. 2 Linggong Road, 116024 Dalian, P. R. China
E-mail: quanaowu@foxmail.com

Chun-an Tang, Ph.D., Professor
School of Civil Engineering, Dalian University of Technology
No. 2 Linggong Road, 116024 Dalian, P. R. China
E-mail: tca@mail.neu.edu.cn

Hongyuan Liu, Ph.D.
School of Engineering and ICT, University of Tasmania, Hobart,
TAS7001, Australia
E-mail: Hong.Liu@utas.edu.au